J|A|C|S
ARTICLES
Published on Web 01/22/2004

Double- and Zero-Quantum NMR Relaxation Dispersion Experiments Sampling Millisecond Time Scale Dynamics in Proteins

Vladislav Yu. Orekhov,*,† Dmitry M. Korzhnev,‡ and Lewis E. Kay‡

Contribution from the Swedish NMR Center at Göteborg University, Box 465, 40530 Göteborg, Sweden, and Protein Engineering Network Centers of Excellence and Departments of Medical Genetics, Biochemistry and Chemistry, The University of Toronto, Toronto, Ontario M5S 1A8, Canada

Received September 19, 2003; E-mail: orov@nmr.se

Abstract: TROSY-based NMR relaxation dispersion experiments that measure the decay of double- and zero-quantum $^{1}H-^{15}N$ coherences as a function of applied ^{1}H and ^{15}N radio frequency (rf) fields are presented for studying millisecond dynamic processes in proteins. These experiments are complementary to existing approaches that measure dispersions of single-quantum ^{15}N and ^{1}H magnetization. When combined, data from all four coherences provide a more quantitative picture of dynamics, making it possible to distinguish, for example, between two-site and more complex exchange processes. In addition, a TROSY-based pulse scheme is described for measuring the relaxation of amide ^{1}H single-quantum magnetization, obtained by a simple modification of the multiple-quantum experiments. The new methodology is applied to a point mutant of the Fyn SH3 domain that exchanges between folded and unfolded states at 25 °C.

Introduction

Dynamics are critical for molecular function. In the case of biological macromolecules, important processes such as folding, ligand binding, enzyme catalysis, and molecular recognition all involve motions that potentially span a wide range of time scales and amplitudes.[1−6] Often these processes rely on transitions to low populated but functionally important states, and an understanding of the relation between structure, dynamics, and function requires, therefore, a thorough characterization of these excited states. Recent advances in solution NMR spectroscopy have facilitated their study. Relaxation dispersion experiments, in which the contributions to line widths from exchange are quantified as a function of the strength of applied radio frequency fields, have been developed to monitor dynamic processes with time scales in the millisecond-to-microsecond regime.[7−9] In some cases these experiments allow the characterization, in a site-specific manner, of the kinetics (rates), thermodynamics (populations), and structural changes (chemical shift differences between states) that are involved in the interconversion,[3,10] providing extremely valuable information.

To date, experiments for the study of millisecond time scale dynamics have focused on the measurement of relaxation properties of single-quantum coherences of backbone amide nitrogen, amide proton, α-carbon, and side chain methyl carbon spins.[2,3,9,11] Figure 1 shows an energy level diagram for an isolated $^{1}H-^{15}N$ spin system, with the frequencies of the single-quantum ^{1}H and ^{15}N transitions indicated by $|\omega_H|$ and $|\omega_N|$, respectively. It is readily apparent that there are two additional transitions, those associated with double- and zero-quantum coherences, that can be studied as well, providing complementary information to the single-quantum measurements. Here we present simple constant-time TROSY-based[12] (Transverse Relaxation Optimized Spectroscopy) CPMG-type (Carr−Purcell−Meiboom−Gill) pulse schemes for measuring $^{1}H-^{15}N$ double- (DQ), zero- (ZQ), and ^{1}H single-quantum (SQ) dispersion profiles and illustrate their utility with an application to a G48M mutant of the Fyn SH3 domain[13] that exchanges between folded and unfolded conformers.

Materials and Methods

Sample Preparation. ^{15}N-labeled, perdeuterated Fyn SH3 domain with Met substituted for Gly at position 48 (G48M) was prepared as described previously,[13] except that the protein was expressed in D_2O

† Göteborg University.
‡ The University of Toronto.

(1) Farrow, N. A.; Zhang, O.; Forman-Kay, J. D.; Kay, L. E. *Biochemistry* **1995**, *34*, 868−878.
(2) Hill, R. B.; Bracken, C.; DeGrado, W. F.; Palmer, A. G. *J. Am. Chem. Soc.* **2000**, *122*, 11610−11619.
(3) Mulder, F. A. A.; Mittermaier, A.; Hon, B.; Dahlquist, F. W.; Kay, L. E. *Nat. Struct. Biol.* **2001**, *8*, 932−935.
(4) Eisenmesser, E. Z.; Bosco, D. A.; Akke, M.; Kern, D. *Science* **2002**, *295*, 1520−1523.
(5) Kay, L. E.; Muhandiram, D. R.; Wolf, G.; Shoelson, S. E.; Forman-Kay, J. D. *Nat. Struct. Biol.* **1998**, *5*, 156−163.
(6) Lee, A. L.; Kinnear, S. A.; Wand, A. J. *Nat. Struct. Biol.* **2000**, *7*, 72−77.
(7) Palmer, A. G.; Kroenke, C. D.; Loria, J. P. *Methods Enzymol.* **2001**, *339*, 204−238.
(8) Skrynnikov, N. R.; Mulder, F. A. A.; Hon, B.; Dahlquist, F. W.; Kay, L. E. *J. Am. Chem. Soc.* **2001**, *123*, 4556−4566.
(9) Ishima, R.; Torchia, D. *J. Biomol. NMR* **2003**, *25*, 243−248.
(10) Korzhnev, D. M.; Karlsson, B. G.; Orekhov, V. Y.; Billeter, M. *Protein Sci.* **2003**, *12*, 56−65.
(11) Loria, J. P.; Rance, M.; Palmer, A. G. *J. Am. Chem. Soc.* **1999**, *121*, 2331−2332.
(12) Pervushin, K.; Riek, R.; Wider, G.; Wüthrich, K. *Proc. Natl. Acad. Sci. U.S.A.* **1997**, *94*, 12366−12371.
(13) Maxwell, K. L.; Davidson, A. R. *Biochemistry* **1998**, *37*, 16172−16182.

10.1021/ja038620y CCC: $27.50

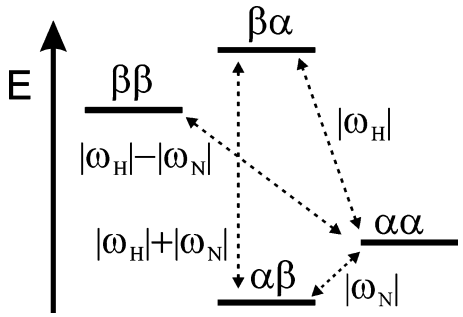

Figure 1. Energy level diagram for a two-spin $^1H-^{15}N$ spin system, with $\gamma_H > 0$, $\gamma_N < 0$, where γ_i is the gyromagnetic ratio of spin i. The symbols α and β correspond to the "up" and "down" orientations of the spins with the first and the second positions denoting proton and nitrogen spin states, respectively. The absolute values of the energies (rad/s) of each of the transitions are indicated (neglecting the very small contribution from J_{NH}).

media and ^{12}C,^2H-glucose was used as the carbon source. The sample used was 0.8 mM protein, 50 mM sodium phosphate, 0.2 mM EDTA, 0.05% NaN_3, pH 7, 10% D_2O. An ^{15}N-labeled, perdeuterated sample of the 63 residue protein L was prepared as before.[14] It is known from previous work that this protein does not show millisecond time scale dynamics, and we have therefore used it as a test of the proposed methodology (see below). The protein L sample conditions were 3 mM protein, 50 mM sodium phosphate, pH 6.0, 0.01% NaN_3, 10% D_2O.

NMR Spectroscopy. All experiments were recorded at 25 °C on Varian Inova spectrometers at field strengths of 11.7, 14.1, and 18.8 T. Briefly, TROSY-based $^1H-^{15}N$ DQ, ZQ, and ^1H SQ dispersion profiles were obtained using spin−echo pulse trains, modified as described in the legend to Figure 2. (In what follows we will refer to these pulse trains as "CPMG-type" or occasionally "CPMG" for brevity, although it is important to stress that the phase cycle of the elements of the train are distinct from those originally reported for the CPMG scheme[15,16]). In this approach chemical exchange dephasing is attenuated as a function of the variable spacing between refocusing pulses applied during a constant time delay, T,[17,18] usually 30 or 40 ms in our experiments. The CPMG field strength, $\nu_{CPMG} = 1/(4\tau_{CPMG})$, where $2\tau_{CPMG}$ is the time between successive refocusing pulses, is varied between approximately 50 and 1000 Hz in the DQ/ZQ experiments and up to 3 kHz in the ^1H SQ profiles (even numbers of pulses used). Peak intensities $I(\nu_{CPMG})$ were measured from a series of typically 10−15 two-dimensional $^1H-^{15}N$ correlation maps and converted to effective decay constants $R_{2,eff}$ according to the relation $R_{2,eff} = -\ln\{I(\nu_{CPMG})/I(0)\}/T$, where $I(0)$ is the corresponding peak intensity when the constant-time CPMG-type element is removed.[17,18] Uncertainties in $R_{2,eff}$ values were obtained on the basis of repeat measurements at three separate ν_{CPMG} values, as described previously[17] (in cases where these errors were less than 2% (5%) for SQ (DQ, ZQ) dispersions, errors of 2% (5%) were assumed). In addition to the TROSY-based $^1H-^{15}N$, DQ, ZQ, and ^1H SQ experiments, additional ^{15}N and ^1H SQ dispersion profiles (non-TROSY) were recorded using pulse schemes described previously.[9,11,18] The total measuring times for each of the complete $^1H-^{15}N$ DQ, ZQ, ^{15}N SQ, and ^1H SQ dispersions were 22, 18, and 22 h (for each of the two SQ experiments), respectively (0.8 mM sample). Relaxation dispersion profiles were fit numerically to a two-site exchange process using in-house-written software relating $R_{2,eff}$ to ν_{CPMG}, where the difference in chemical shifts between the exchanging states is given by $\Delta\omega_{ZQ}$ or $\Delta\omega_{DQ}$ for zero- or double-quantum dispersions, as described below. (Alternatively, dispersion profiles can be fit using the Carver−Richards equation,[19] for example, eqs 3−8 of Millet et al.[20]).

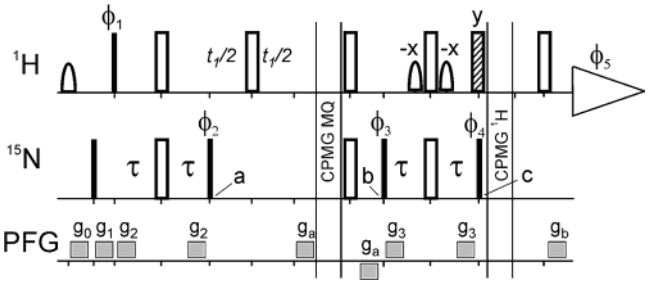

Figure 2. Pulse sequence for measuring relaxation dispersion profiles of zero-quantum, double-quantum, and ^1H spin-state selective coherences. All narrow, filled (wide, open) rectangular radio frequency pulses are applied with flip angles of 90° (180°), respectively, along the x axis, unless indicated otherwise. The ^1H and ^{15}N carriers are positioned at water and at 119 ppm, respectively, with the ^1H carrier jumped to 8.1 ppm for the duration of either constant-time CPMG-type blocks,[17,18] denoted by CPMG MQ and CPMG ^1H. Note that when the relaxation properties of zero-quantum and double-quantum coherences are measured the CPMG ^1H element is removed, while the CPMG MQ period is omitted when ^1H single-quantum dispersion profiles are recorded. Field strengths of 25 and 6.3 kHz are employed for ^1H and ^{15}N pulses, respectively, except as discussed below. At the beginning of the pulse scheme water magnetization is destroyed by the water selective EBURP-1 pulse[36] (6 ms) followed by the gradient g_0. Further solvent suppression is achieved with the water-gate element[37] between points b and c, which makes use of rectangular water-selective 90° pulses (1.2 ms). The delay τ is set to 2.7 ms. The duration and strengths of the field gradient pulses, which are all applied along the Z axis, are g_a = (0.15 ms, 21.57 G/cm), g_b = (0.15 ms, −47.48 G/cm), g_0 = (0.3 ms, 41 G/cm), g_1 = (0.1 ms, 5.1 G/cm), g_2 = (1.9 ms, 1 G/cm), and g_3 = (0.80 ms, 4 G/cm), with gradients g_a and g_b used to select the desired coherence transfer pathway.[24,38] The phase cycle employed is $\phi_1 = \{2(x,-x), 2(y,-y)\}$, $\phi_2 = \{2(-y), 2(y), 2(-x), 2(x)\}$, $\phi_3 = \{4(x), 4(-x)\}$, $\phi_4 = \{4(y), 4(-y)\}$, and $\phi_5 = \{x, -x, -x, x, -x, x, x, -x\}$. Phase sensitive quadrature detection in the indirect dimension is achieved by recording a second free induction decay (FID) for each t_1 increment with the sign of gradients g_a inverted and the ^1H 180° pulse immediately before point c (hatched) omitted. In practice, composite pulses $90°_x180°_y90°_x$ and $90°_x180°_x90°_x$ are used for the first and second FIDs, respectively. The phase cycle and gradient strengths described above are used for measuring zero-quantum and spin-state selective proton single-quantum relaxation dispersion profiles. In the case where double-quantum profiles are obtained, g_a = 26.43 G/cm, phase ϕ_4 is inverted, and $\phi_5 = \{-x, x, x, -x\}$. The MQ CPMG type element makes use of composite pulses of the form $90_{\psi-\pi/2}240_{\psi}90_{\psi-\pi/2}$[39] for MQ CPMG frequencies up to 550 Hz, with hard pulses, $180°_{\psi}$, used for higher frequencies. The pulses are applied simultaneously on ^1H and ^{15}N rf channels. The following CPMG frequency dependent phase scheme is employed: XY4 (0−55 Hz), $\psi = \{x, y, x, y\}$; XX (55−275 Hz), $\psi = \{x\}$; and XY8 for higher frequencies, $\psi = \{x, y, x, y, y, x, y, x\}$, where it is understood that for each successive 180° pulse in the CPMG train the phase ψ is incremented. (In cases where the number of refocusing pulses, k, during a pulse train does not coincide with the complete phase cycle ψ, only the first k elements in the cycle are used. It is noteworthy that for frequencies in excess of 275 Hz, i.e., when the XY8 cycle is used, the number of pulses is set to a multiple of 4.) For the proton CPMG refocusing sequence, labeled CPMG ^1H, the XY16 scheme, $\psi = \{x, y, x, y, y, x, y, x, -x, -y, -x, -y, -y, -x, -y, -x\}$ with ^1H $180°_{\psi}$ hard rf pulses, is employed (pulses applied in multiples of 4). Each of the CPMG elements is of constant duration, T, as described previously for the measurement of ^{15}N and ^{13}C dispersion profiles.[8,18] Typically T values that decrease the signal by approximately a factor of 2 (relative to $T = 0$) are employed.

Finally, it is important to mention that highly deuterated samples are key in applications which record dispersion profiles of $^1H-^{15}N$ DQ, ZQ, and ^1H SQ coherences. In the case of protonated samples (i) homonuclear scalar coupled transfer of magnetization from amide ^1H

(14) Scalley, M. L.; Yi, Q.; Gu, H.; McCormack, A.; Yates, J. R.; Baker, D. *Biochemistry* **1997**, *36*, 3373−82.
(15) Carr, H. Y.; Purcell, E. M. *Phys. Rev.* **1954**, *4*, 630−638.
(16) Meiboom, S.; Gill, D. *Rev. Sci. Instrum.* **1958**, *29*, 688−691.
(17) Mulder, F. A. A.; Skrynnikov, N. R.; Hon, B.; Dahlquist, F. W.; Kay, L. E. *J. Am. Chem. Soc.* **2000**, *123*, 967−975.
(18) Tollinger, M.; Skrynnikov, N. R.; Mulder, F. A. A.; Forman-Kay, J. D.; Kay, L. E. *J. Am. Chem. Soc.* **2001**, *123*, 11341−11352.
(19) Carver, J. P.; Richards, R. E. *J. Magn. Reson.* **1972**, *6*, 89−105.

to aliphatic protons and (ii) ^{1}H−^{1}H transverse cross-relaxation, both of which can occur during the CPMG period in a ν_{CPMG}-dependent manner, complicate the extraction of accurate exchange parameters.[9]

Results and Discussion

The experimental schemes for recording TROSY-based ^{1}H−^{15}N DQ, ZQ, and ^{1}H SQ CPMG-type dispersion profiles are illustrated in Figure 2. The sequences are similar to an elegant zero-quantum TROSY-based NOESY experiment described by Pervushin and co-workers[21] and will therefore be described only briefly. Amide proton magnetization at the start of the experiment is converted into the sum of zero- and double-quantum coherences, $ZQ_- + ZQ_+ + DQ_- + DQ_+$, at point *a*. Here multiple-quantum coherences are defined in the usual way, as the products of single-quantum ^{1}H and ^{15}N coherences, i.e., $ZQ_\pm = H_\mp N_\pm$ and $DQ_\pm = H_\pm N_\pm$, where $I_\pm = I_X \pm iI_Y$, and I_X, I_Y are the usual Cartesian product operators.[22] The ^{1}H 180° pulse in the middle of the evolution period, t_1, exchanges double- and zero-quantum coherences, so that the net acquired phase for all coherences immediately prior to gradient g_a is the result of ^{15}N chemical shift evolution. Note that in some cases it may be desirable to record ^{1}H−^{15}N DQ or ZQ chemical shifts instead,[23] and this can be easily accomplished as well by omission of the ^{1}H refocusing pulse described above. The pair of field gradients, g_a, and the simultaneous 180° pulses on both nuclei between them are used to encode a desired pair of coherences, either $ZQ_\pm$ or $DQ_\pm$. The element entitled "CPMG MQ", placed immediately after the first g_a gradient, is a constant-time evolution period, of duration *T*, during which time simultaneous ^{1}H and ^{15}N 180° pulse pairs are applied. This leads to the attenuation of the selected coherence due to relaxation and conformational exchange. Subsequently, the multiple-quantum plus and minus coherences (for example, $ZQ_\pm$) are quantitatively transferred to transverse relaxation optimized, single-quantum spin selective states, DQ_+,ZQ_- to $H_+(1-2N_z)$ and DQ_-,ZQ_+ to $H_-(1-2N_z)$, during the interval between points *b* and *c*, as described by Pervushin et al.[21] The spin-state selective TROSY magnetization is decoded by the last gradient g_b and detected using the enhanced sensitivity approach described previously.[24] Note that if ^{1}H single-quantum dispersions are to be recorded, the constant-time element, CPMG ^{1}H, is inserted as shown (see Figure 2), with the CPMG MQ scheme removed.

It is worth mentioning that the DQ/ZQ sequence is a factor of 2 less sensitive than the corresponding enhanced sensitivity ^{15}N single-quantum experiment (but only $\sqrt{2}$ less sensitive than an unenhanced single-quantum experiment), neglecting relaxation, since only half the signal, corresponding either to $ZQ_\pm$ or $DQ_\pm$, is retained. However, the relaxation properties of ^{1}H−^{15}N DQ/ZQ coherences can be quite favorable in highly deuterated proteins,[25] at least in the absence of chemical exchange, and recording the TROSY ^{1}H component during acquisition is also advantageous. In applications that we have considered to date, sensitivity has not been an overwhelming issue. It is also worth noting that TROSY-based DQ and ZQ dispersion schemes *are no less sensitive* than their non-TROSY counterparts. In the TROSY version of the experiment either DQ or ZQ coherences are transferred to the slowly relaxing ^{1}H multiplet component, while in the non-TROSY version the signal is distributed over both multiplet components. In this sense the TROSY version is preferred since it benefits from more favorable relaxation during acquisition.

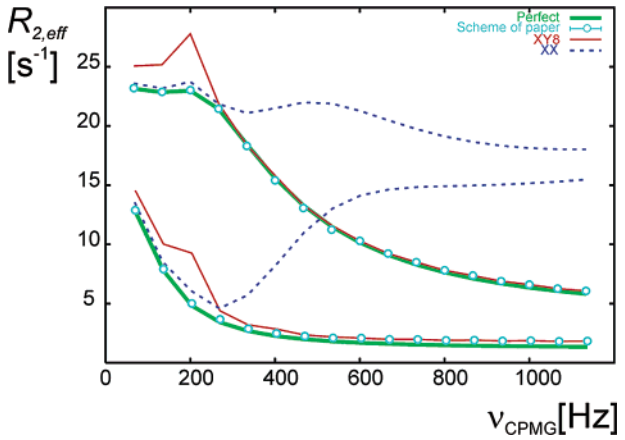

Figure 3. Relaxation dispersion profiles obtained by density matrix simulations of a two-spin ^{1}H−^{15}N spin system using different CPMG schemes. DQ dispersion profiles are shown in the upper four traces, while the ZQ profiles are the bottom four. A two-site exchange process has been assumed, described with exchange parameters $k_{ex} = 400$ s^{-1}, $p_B = 0.05$, $\Delta\omega_H = 0.26$ ppm, and $\Delta\omega_N = 0.44$ ppm (^{1}H ppm). Relaxation of each density element (dipolar and chemical shift anisotropy interactions, 600 MHz spectrometer frequency) is included using the Lipari−Szabo spectral density[40,41] with S^2 (order parameter squared) = 0.8, τ_e (correlation time for fast motions) = 10 ps, and τ_R (overall tumbling correlation time) = 4 ns. Relaxation in each of the exchanging states is assumed to be the same. The simulations have been performed in a space of 32 Cartesian operators (16 for each state), necessary for describing exchange in such a system. Dispersions obtained with ideal, short on-resonance pulses are in green; dispersions generated with an XY8 cycle of CPMG pulses,[26,27] with ^{1}H, ^{15}N 180° pulse widths of 14, 80 μs, respectively, and ^{1}H, ^{15}N offsets of 0, 500 Hz, respectively, are in red; dispersions calculated using the same pulse widths and offsets as for XY8 but with all pulses of constant phase (X) are indicated with blue dashes; and, finally, dispersions generated using the CPMG frequency dependent scheme described in the text (see legend to Figure 2) are shown by blue circles (same offsets and pulse widths as for XY8 and X CPMG schemes). Pulse miscalibrations and the effects of radio frequency inhomogeneity are not included in the simulations. However, such effects are compensated experimentally by using pulses of the type $90_{\psi-\pi/2}240_{\psi}90_{\psi-\pi/2}$[39] (see legend to Figure 2).

The development of the DQ/ZQ dispersion (and ^{1}H SQ dispersion) experiments is complicated by the fact that both *X* and *Y* components of magnetization must be preserved during the CPMG MQ element. For this purpose we use *XY*-type phase cycled sequences,[26,27] described in the legend to Figure 2, that were originally designed for such applications but in the case where magnetization derives from an isolated nucleus (i.e., uncoupled spin). These schemes compensate for small imperfections in radio frequency (rf) pulses, caused by their finite length (offset effects) and rf inhomogeneity/pulse miscalibration. In a series of computer simulations and test experiments the compensation properties of such schemes were explored in some detail (see below). Substantial artifacts (artificially high relax-

(20) Millet, O.; Loria, J. P.; Kroenke, C. D.; Pons, M.; Palmer, A. G. *J. Am. Chem. Soc.* **2000**, *122*, 2867−2877.
(21) Pervushin, K. V.; Wider, G.; Riek, R.; Wüthrich, K. *Proc. Natl. Acad. Sci. U.S.A.* **1999**, *96*, 9607−9612.
(22) Ernst, R. R.; Bodenhausen, G.; Wokaun, A. *Principles of Nuclear Magnetic Resonance in One and Two Dimensions*; Oxford University Press: Oxford, 1987.
(23) Pervushin, K. *J. Biomol. NMR* **2001**, *20*, 275−285.
(24) Kay, L. E.; Keifer, P.; Saarinen, T. *J. Am. Chem. Soc.* **1992**, *114*, 10663−10665.
(25) Andersson, P.; Gsell, B.; Wipf, B.; Senn, H.; G., O. *J. Biomol. NMR* **1998**, *11*, 279−288.
(26) Simbrunner, J.; Stollberger, R. *J. Magn. Reson. Ser. B* **1995**, *109*, 301−309.
(27) Gullion, T.; Baker, D. B.; Conradi, M. S. *J. Magn. Reson.* **1990**, *89*, 479−484.

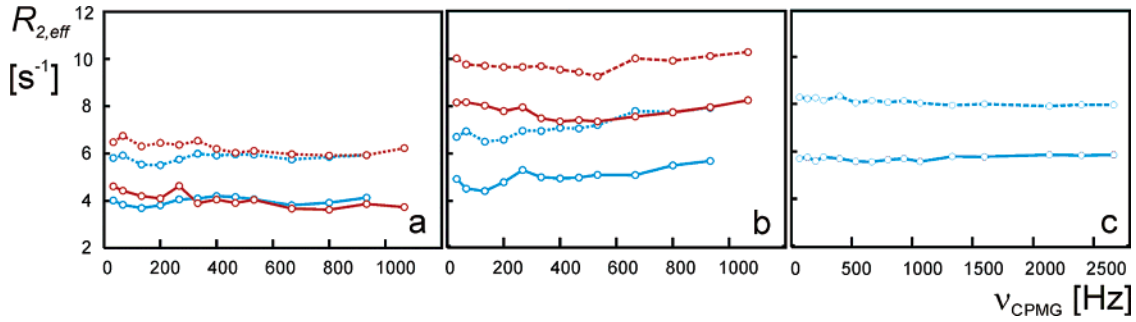

Figure 4. Relaxation dispersion ZQ (a), DQ (b), and ^{1}H SQ (c) profiles for Ala 33 (dashed lines) and Phe 20 (solid lines) of protein L, recorded using the schemes of Figure 2. Data at 500 and 800 MHz are indicated in blue and red, respectively. The standard deviation of $R_{2,eff}$ values is always less than 0.45 s^{-1} for each dispersion shown and averages 0.22, 0.35, and 0.12 s^{-1} for ZQ, DQ, and ^{1}H SQ coherences. Errors in individual $R_{2,eff}$ values are less than 0.1 s^{-1} and are not shown.

ation rates) were observed at certain CPMG frequencies, in a manner dependent on the type of phase cycling employed. For example, at frequencies close to $2J_{NH}$ (J_{NH}), where J_{NH} is the single bond ^{1}H−^{15}N coupling constant, use of the XY8 (XY4) scheme led to inflated transverse relaxation rates in experiments or in computations which included pulse imperfections of the type described above. In contrast, artifacts were not observed at ν_{CPMG} values of ∼100, 200 Hz, for example, when pulses of phase X were applied. At higher frequencies, however, the use of X pulses leads to rapid signal deterioration since only X magnetization is preserved in this case. Therefore, a hybrid scheme in which different phase cycles are employed depending on the CPMG frequency has been developed. Further improvement, observed in both simulations and experiment, was achieved by substituting hard 180°$_\phi$ pulses in the CPMG element with composite pulses of the form $90_{\phi+\pi/2}240_\phi90_{\phi+\pi/2}$ (providing good compensation for offset effects and some compensation with respect to pulse imperfections[28]). The details of the final frequency-dependent phase scheme for the MQ CPMG element is given in the legend to Figure 2. Note that the lengthy composite pulses (90−240−90) are only used at low CPMG frequencies so that they do not impose limitations on the highest CPMG frequency that is possible for measuring MQ dispersions relative to the ^{15}N single-quantum experiment. Finally, in the case where ^{1}H dispersions are recorded, an XY16-based CPMG element[26,27] is used so that both *X* and *Y* magnetization can be ultimately detected, leading to sensitivity improvements of $\sqrt{2}$ over the corresponding scheme where only a single component (*X* or *Y*) is observed.

Figure 3 illustrates some of the artifacts in the DQ/ZQ dispersion profiles, discussed above, that are associated with different CPMG schemes. DQ (upper four traces) and ZQ (bottom four traces) dispersions have been calculated assuming a two-site exchange process described with exchange parameters k_{ex} (sum of forward and reverse exchange rates) = 400 s^{-1}, p_B (population of the minor species) = 0.05, $\Delta\omega_H$ = 0.26 ppm, and $\Delta\omega_N$ = 0.44 ppm (all $\Delta\omega_i$ values listed here and in what follows are in ^{1}H ppm). Complete density matrix calculations for a two-spin spin system have been used, including the effects of relaxation and chemical exchange, modeled as described in the legend to Figure 3. Pulse widths (180°) have been set to 80 and 14 μs for ^{15}N and ^{1}H, respectively, which are about average for triple-resonance probe heads on our spectrometers. The dispersions in green correspond to those obtained for a peak that is on-resonance in the nitrogen dimension (generated with very short ^{15}N 180° pulse widths), used as a control in what follows. Dispersion profiles calculated based on an XY8 scheme (red) or a CPMG sequence with all pulses of constant phase (blue dashes) show significant errors in the case where spins are off-resonance. Here we have assumed an offset in the ^{15}N dimension of 500 Hz (80 μs ^{15}N 180° pulse width). In particular, errors are extreme when ^{15}N pulses of constant phase are employed since cumulative errors resulting from pulse offset effects at high ν_{CPMG} rates essentially dephase half the signal. This can be understood by noting that DQ (ZQ) coherence can be written as $H_XN_X - H_YN_Y$ ($H_XN_X + H_YN_Y$) and recalling that imperfections in ^{15}N refocusing pulses applied along the *X*-axis effectively destroy N_Y. In contrast, when the phase scheme that varies with CPMG frequency suggested above is employed, dispersions that are free of artifacts are obtained (blue circles).

The pulse sequences were first tested on a sample of perdeuterated protein L, which is known from our previous studies to show no exchange line broadening.[29] Relatively flat relaxation dispersions for zero- (Figure 4a), double- (Figure 4b), and spin-state selective single-quantum ^{1}H coherences (Figure 4c) were obtained for all amide signals, illustrated for a pair of typical residues, Ala 33 and Phe 20, with data at 500 and 800 MHz, 25 °C, indicated in blue and red, respectively. Note that the DQ rates increase significantly with spectrometer field relative to the ZQ rates (compare blue with red in (b) and in (a)), due to the partial cancellation of relaxation fields from ^{1}H and ^{15}N chemical shift anisotropy interactions in the case of ZQ coherences.[21,30] The largest deviation of $R_{2,eff}$ from the mean $R_{2,eff}$ for each of the dispersions illustrated in the figure is less than 0.8 s^{-1} (average over all dispersions of less than 0.5 s^{-1}). The standard deviations of the relaxation rates in most of the dispersions measured for protein L, 25 °C, were less than 0.5 s^{-1}. Very similar deviations were obtained for dispersions recorded at 5 °C, indicating that the errors resulting from pulse imperfections do not scale with molecular size.

Figure 5 shows relaxation dispersion profiles (a, e ZQ; b, f DQ; c, g ^{1}H SQ; d, h ^{15}N SQ) for the amide groups of Asp 9 (Figure 5a−d) and Thr 47 (Figure 5e−h) in the G48M mutant of the Fyn SH3 domain, 25 °C. Dispersion profiles for the great majority of residues in the protein are of equal quality to the ones in the figure. In a very recent study a series of seven mutants of the Fyn SH3 domain at position 48 have been

(28) Freeman, R.; Kempsell, S. P.; Levitt, M. H. *J. Magn. Reson.* **1980**, *38*, 453−479.
(29) Millet, O.; Mittermaier, A.; Baker, D.; Kay, L. E. *J. Mol. Biol.* **2003**, *329*, 551−563.
(30) Korzhnev, D. M.; Billeter, M.; Arseviev, A. S.; Orekhov, V. Y. *Prog. Nucl. Magn. Reson. Spectrosc.* **2001**, *38*, 197−266.

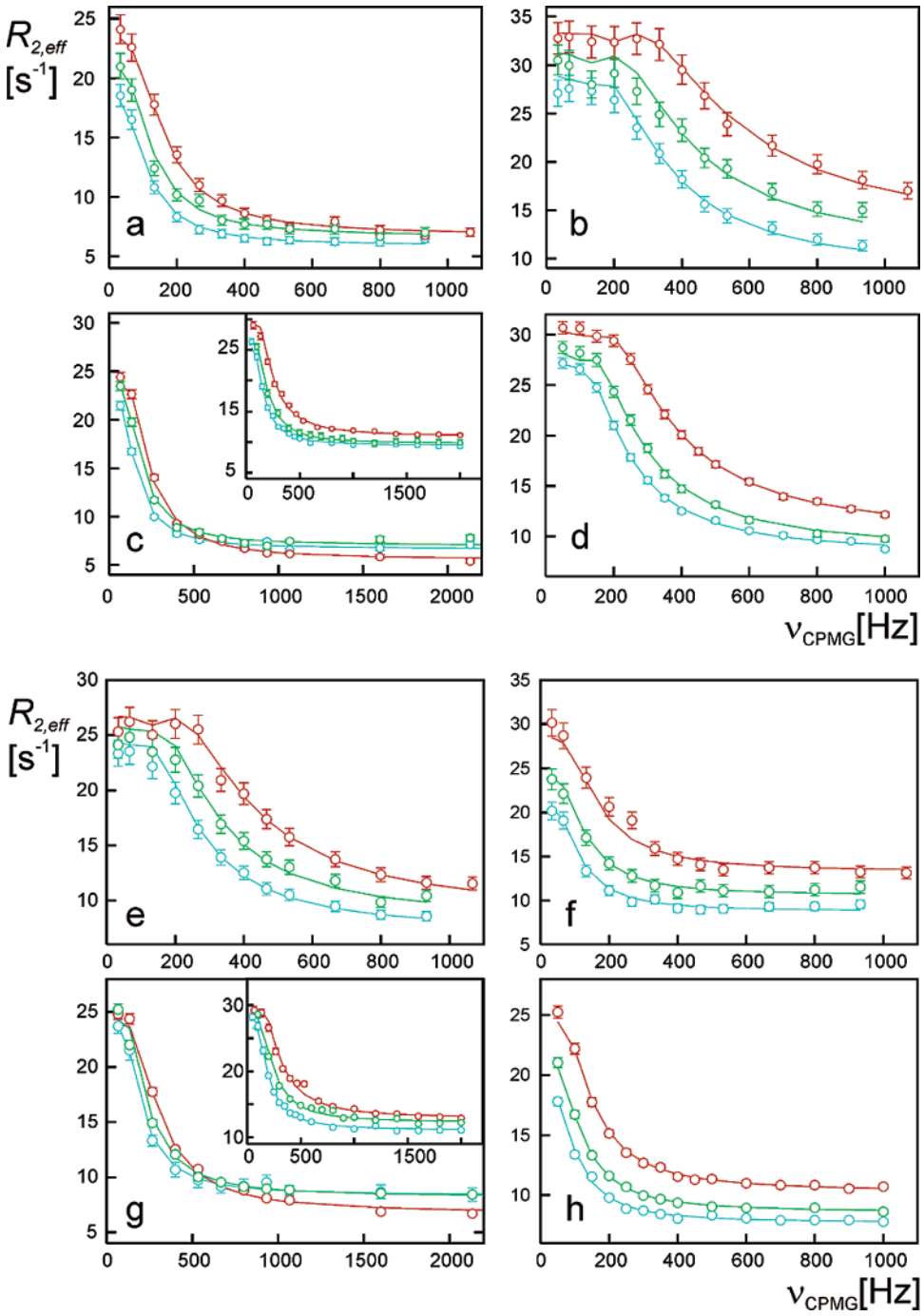

Figure 5. Relaxation dispersion profiles for Asp 9 (a−d) and Thr 47 (e−h) of the G48M Fyn SH3 domain mutant (0.8 mM in protein, 25 °C). Profiles of the relaxation rate $R_{2,eff}$ as a function of ν_{CPMG} for ZQ, DQ, and ^{1}H-TROSY[12] coherences, measured using the pulse sequence presented in Figure 2, are shown in frames a (e), b (f), and c (g), respectively. ^{15}N dispersions measured using the standard relaxation compensated,[11] constant-time scheme[17,18] are shown in frame d (h). Individual measurements, shown as circles with error bars, and theoretical fits (lines), are presented for three magnetic fields 11.7, 14.1, and 18.8 T, color-coded blue, green, and red, respectively. For comparison, ^{1}H dispersions measured using a previously published non-TROSY scheme[9] are shown in the inset to frames c and g. All dispersions presented in the figure (except for the non-TROSY ^{1}H data) were fit together, on a per-residue basis using a two-site exchange model.[19] In this approach 12 dispersion curves (three fields, ZQ, DQ, ^{1}H, and ^{15}N) corresponding to 152 data points are fit to global values of k_{ex} and p_B, along with a separate intrinsic relaxation rate constant for each dispersion (12 rates) and a single $\Delta\omega_i$ value for each set of profiles of a given type (for example, DQ) recorded at the three fields ($4\Delta\omega_i$ values in total), so that for each residue (12 dispersion curves) 18 fitting parameters are employed (134 degrees of freedom). Values of 369 ± 16 (326 ± 14) s^{-1} and 5.6 ± 0.1 (5.5 ± 0.2)% for the exchange rate and population of the minor state, respectively, are obtained for Asp 9 (Thr 47). The differences (absolute values) between precession frequencies in the two states (folded/unfolded) for ^{1}H, ^{15}N, ZQ, and DQ coherences are (all ^{1}H ppm) 0.27 ± 0.003 (0.36 ± 0.005), 0.45 ± 0.005 (0.17 ± 0.002), 0.18 ± 0.004 (0.52 ± 0.014), and 0.69 ± 0.02 (0.19 ± 0.006), respectively. The intrinsic transverse relaxation rates in both states were assumed equal in all fits. Although this is certainly not the case for a folding/unfolding transition (differences in R_2 values estimated on the order of 3.5 s^{-1}, based on results for the drkN SH3 domain[1]), simulations indicate that essentially no error is introduced by the assumption of equal rates, due to the highly skewed populations in this system. See for example, Millet et al.[20]

examined, including G48M, and kinetic parameters were measured from ^{15}N relaxation dispersion experiments. The exchange parameters obtained from a two-state analysis of the data measured at 25 °C correlate remarkably well with stopped-flow folding and unfolding rates generated as a function of denaturant,[31] providing strong evidence that the process that we are observing is a folding/unfolding event.

Data for ^{1}H, ^{15}N, and ZQ, DQ coherences, measured at 11.7, 14.1, and 18.8T, are well fit assuming a two-site exchange process with reduced χ^2 values (χ^2/number of degrees of freedom) ≤ 1; see Figure 5. In each fit all of the dispersions for a given residue were considered together, the chemical shift differences in the two states, $|\Delta\omega|$, were adjusted independently for every coherence, and the folding/unfolding rates and populations of the two states fit globally. The following $|\Delta\omega_i|$ values were obtained from the fit of Asp 9 (Thr 47): $|\Delta\omega_H| = 0.27 \pm 0.003$ (0.36 ± 0.005), $|\Delta\omega_N| = 0.45 \pm 0.005$ (0.17 ± 0.002), $|\Delta\omega_{ZQ}| = 0.18 \pm 0.004$ (0.52 ± 0.014), $|\Delta\omega_{DQ}| = 0.69 \pm 0.02$ (0.19 ± 0.006) (all numbers in ^{1}H ppm). The absolute sign of $\Delta\omega_i$ is not available from these experiments, and we therefore report absolute values. The signs of the shift differences can be obtained, however, by comparing peak shifts in single-quantum and multiple-quantum data sets.[32] Such an analysis has been performed for this domain, and the sign of the $\Delta\omega_N$ values are consistent with an unfolding process.

It is worth noting that $|\Delta\omega_{ZQ}|$ and $|\Delta\omega_{DQ}|$ can be constructed from $\Delta\omega_H$ and $\Delta\omega_N$ according to $|\Delta\omega_{DQ}| = |\Delta\omega_H + \Delta\omega_N|$ and $|\Delta\omega_{ZQ}| = |\Delta\omega_H - \Delta\omega_N|$, and that $|\Delta\omega_{DQ}| > |\Delta\omega_{ZQ}|$ when $\Delta\omega_H\Delta\omega_N > 0$. Therefore, the relative signs of $\Delta\omega_H$ and $\Delta\omega_N$ are available from an analysis of double- and zero-quantum dispersions, as described previously.[33,34] For example, in the case of Asp 9, the $\Delta\omega_i$ values listed above imply that $\Delta\omega_H$ and $\Delta\omega_N$ have the same sign, while for Thr 47 $\Delta\omega_H\Delta\omega_N < 0$. Moreover, the relations between $|\Delta\omega_{ZQ}|$, $|\Delta\omega_{DQ}|$, $\Delta\omega_H$, and $\Delta\omega_N$ listed above provide a check of the consistency of the extracted chemical shift differences, if each of the values is treated as a variable in fits (as was done here). The values of $\Delta\omega_i$ for Asp 9 are in excellent agreement as are those for Thr 47. In addition, k_{ex} and p_B, obtained from fits of the Asp 9 and Thr 47 dispersions, are very similar, $k_{ex} = 369 \pm 16$, 326 ± 14 s^{-1} and $p_B = 5.6 \pm 0.2$, 5.5 ± 0.2%.

Not surprisingly, nearly the same exchange parameters are obtained by interchanging ^{1}H dispersion data measured using the TROSY (Figure 4c,g) and non spin-state selective CPMG[9] experiments (Figure 4c,g inset). However, noticeable differences between the intrinsic relaxation rates (plateau at the high CPMG rates) are clearly seen for the two data sets, even for a small protein, such as the Fyn SH3 domain. These rates become slower at higher B_o field in the case of the TROSY data (compare 500 vs 800 MHz, Figure 4c and 4g) due to the improved cancellation of dipole/chemical shift anisotropy interactions with increasing B_o, an effect that is well documented in the literature.[12] The improvements in relaxation times, translate, of course, to sensitivity gains and can be quite considerable for applications involving medium-sized proteins, considering that constant-time relaxation periods on the order of 20−40 ms are employed in these experiments.

This study significantly extends the work of Kloiber and Konrat[33] and Bodenhausen and co-workers,[34] showing that large differences in relaxation rates of double- and zero-quantum coherences in the free precession limit (the $\nu_{CPMG} = 0$ point of the dispersion curves recorded here) could be used to establish the existence of chemical exchange and that, further, the relative signs of $\Delta\omega_H$ and $\Delta\omega_N$ could be obtained from a comparison of these multiple-quantum decay rates. More recently, Palmer and co-workers have provided guidelines of when MQ or SQ coherences might be most sensitive to chemical exchange.[35] The techniques presented here add to the set of dispersion experiments that can be obtained for an isolated ^{1}H−^{15}N two-spin system. Analysis of the four dispersion data sets will facilitate the extraction of more accurate exchange parameters than is possible from ^{15}N or ^{1}H single-quantum measurements alone. Cases where inconsistent dynamics parameters are obtained for the different dispersions from individual fits using a two-site exchange model (or poor-quality fits when all are analyzed together) point to exchange kinetics involving more than two states. It is clear that these experiments will be a valuable addition to the existing methodology for studying millisecond dynamic processes in proteins.

Acknowledgment. The authors thank Dr. Ariel A. Di Nardo for kindly providing a sample of perdeuterated, ^{15}N-labeled G48M Fyn SH3 domain, Dr. Karin Kloiber and Irina Bezsonova for assistance in the production of labeled protein L, and Dr. Dennis Torchia for a critical evaluation of the manuscript prior to publication. This work was supported by Grant 621-2001-3095 from the Swedish Research Council (V.Y.O.), by Grant D1/341 from STINT (V.Y.O.), and by funding from the Canadian Institutes of Health Research (L.E.K.). NMR experiments were performed jointly at the Swedish NMR Center and at the NMR Center of the University of Toronto. L.E.K. holds a Canada Research Chair in Biochemistry.

JA038620Y

(31) Di Nardo, A. A.; Korzhnev, D. M.; Zarrine-Afsar, A.; Kay, L. E.; Davidson, A. R. Submitted for publication.
(32) Skrynnikov, N. R.; Dahlquist, F. W.; Kay, L. E. *J. Am. Chem. Soc.* **2002**, *124*, 12352−12360.
(33) Kloiber, K.; Konrat, R. *J. Biomol. NMR* **2000**, *18*, 33−42.
(34) Fruh, D.; Tolman, J. R.; Bodenhausen, G.; Zwahlen, C. *J. Am. Chem. Soc.* **2001**, *123*, 4810−4816.
(35) Wang, C. Y.; Palmer, A. G. *J. Biomol. NMR* **2003**, *24*, 263−268.
(36) Geen, H.; Freeman, R. *J. Magn. Reson.* **1991**, *93*, 93−141.
(37) Piotto, M.; Saudek, V.; Sklenar, V. *J Biomol. NMR* **1992**, *2*, 661−5.
(38) Schleucher, J.; Sattler, M.; Griesinger, C. *Angew. Chem., Int. Ed. Engl.* **1993**, *32*, 1489−1491.
(39) Freeman, R.; Kempsell, S. P.; Levitt, M. H. *J. Magn. Reson.* **1980**, *38*, 453−479.
(40) Lipari, G.; Szabo, A. *J. Am. Chem. Soc.* **1982**, *104*, 4559−4570.
(41) Lipari, G.; Szabo, A. *J. Am. Chem. Soc.* **1982**, *104*, 4546−4559.